Sensors & Actuators: B. Chemical 320 (2020) 128442

Contents lists available at ScienceDirect

Sensors and Actuators B: Chemical

journal homepage: www.elsevier.com/locate/snb

Coaxial microneedle-electrode for multichannel and local-differential recordings of neuronal activity

Shinnosuke Idogawa[a], Koji Yamashita[a], Yoshihiro Kubota[a], Hirohito Sawahata[b], Rioki Sanda[a], Shota Yamagiwa[a], Rika Numano[c,d], Kowa Koida[d,e], Takeshi Kawano[a,*]

[a] Department of Electrical and Electronic Information Engineering, Toyohashi University of Technology, Toyohashi, 441-8580, Japan
[b] Department of Industrial Engineering, Mechanical and Control Engineering Course, National Institute of Technology, Ibaraki College, Ibaraki, 312-8508, Japan
[c] Department of Applied Chemistry and Life science, Toyohashi University of Technology, Toyohashi, 441-8580, Japan
[d] Electronics-Inspired Interdisciplinary Research Institute, Toyohashi University of Technology, Toyohashi, 441-8580, Japan
[e] Department of Computer science and Engineering, Toyohashi University of Technology, Toyohashi, 441-8580, Japan

ARTICLE INFO

Keywords:
Microelectrode
Neural recording
Multichannel recording
Differential recording

ABSTRACT

Electrophysiological recording requires low invasive electrode geometry in the tissue and high-quality signal acquisitions. Here we propose a < 10-μm diameter coaxial cable–inspired needle electrode, which consists of a core electrode in the needle surrounded by another shell electrode. The neuronal recording capability of these electrodes was confirmed by multichannel recording of a mouse cortex *in vivo*. Given that the shell electrode played the role of a reference electrode, the coaxial electrode also enabled a differential recording at the local area within the tissue. Compared to the recording without the referenced shell electrode, the differential recording demonstrated a twofold higher signal-to-noise ratio, while the firing rate increased. These results suggest that the coaxial microneedle-electrode will provide high-quality neuronal signals in electrophysiological recordings including *ex vivo* and *in vitro* applications, similar to the *in vivo* recording.

1. Introduction

The electrophysiological methodology is used in neuroscience and medical applications as well as brain-machine interface technology due to its advantage of having a higher spatiotemporal resolution than other methodologies. While cortical surface potentials such as electrocorticographic signals can be recorded with film-like electrodes [1], devices based on needle-like electrodes that can penetrate the brain tissue present a powerful tool for acquiring subcortical neuronal activities, including local field potential (LFP) and spike signals, with a high spatiotemporal resolution [2].

With recent advances in microelectromechanical system technology, photolithography–based patterning and etching processes have been used to enable penetrative microscale needle-electrode devices [3,4]. The advantages of the attendant fabrication technology include the integration of a large number of electrodes and the geometric miniaturization of each needle [3,5]. However, the tissue penetration of needles with a geometry of ~50 μm can induce the blood–brain barrier breach [6], while needles of over 20 μm can induce a disruption of the local communication among the glia [7]. One means of resolving this issue is to reduce the needle's geometry to less than 10 μm, which will ensure that the tissue suffers no major traumatic injury [8,9]

With this in mind, we propose a vapor–liquid–solid (VLS) method based on silicon growth technology to fabricate microscale needle-electrodes with diameters of less than 7 μm [10,11] as well as various nanoneedle-electrodes [12,13]. However, the number of recording channels of the needle electrode was limited, with each needle electrode having one recording channel at the needle's tip. Moreover, due to the small area of the recording sites (e.g., < 160 μm^2 [10]), further improvements to the quality of the recorded neuronal signals in terms of, for example, signal-to-noise ratio (SNR) are necessary.

We explore a coaxial-cable-inspired needle-electrode device that consists of individual needles inserted with two channel electrodes (Fig. 1a). This includes a core electrode which is surrounded by a tubular insulating layer and a tubular shell electrode that surrounds the core electrode. We also performed multichannel recording of neuronal activities via the core and shell electrodes (Fig. 1b). In addition, given that the shell electrode can play a role as a reference electrode, differential recordings at the local area within the tissue were performed to explore potential improvements in the quality of the neural recording

* Corresponding author at: Department of Electrical and Electronic Information Engineering, Toyohashi University of Technology, 1-1 Hibarigaoka Tempaku-cho, Toyohashi, Aichi, 441-8580, Japan.
E-mail address: kawano@ee.tut.ac.jp (T. Kawano).

https://doi.org/10.1016/j.snb.2020.128442
Received 17 April 2020; Received in revised form 5 June 2020; Accepted 8 June 2020
Available online 10 June 2020
0925-4005/

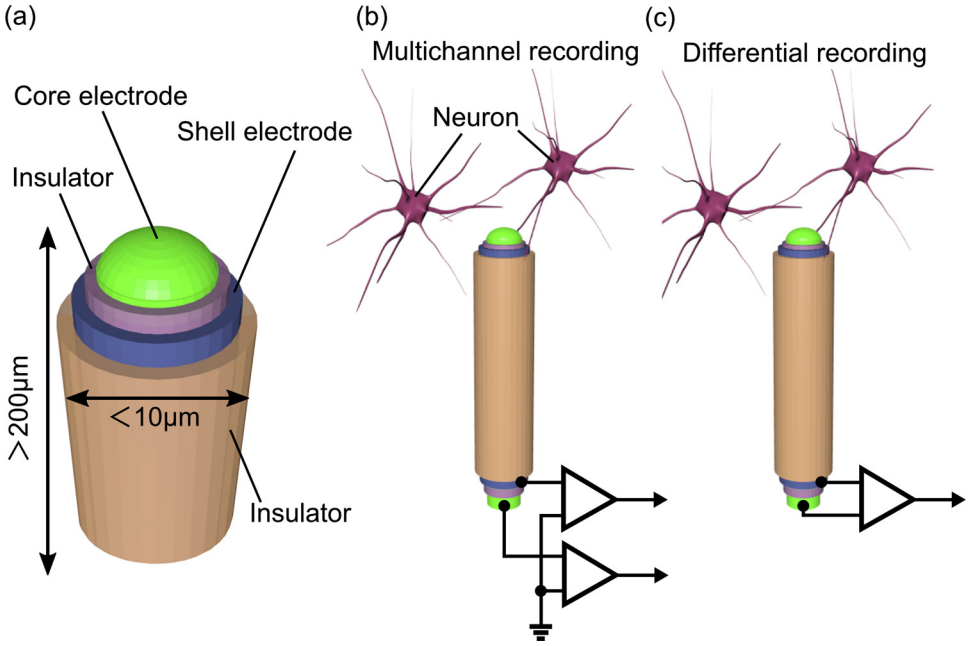

Fig. 1. Coaxial microneedle-electrodes for use in multichannel and local-differential recordings of neuronal activity. (a) Schematic diagram of the coaxial microneedle-electrode; (b) Schematic diagram of multichannel recording. Here, the core electrode and the shell electrode in the needle were connected with each signal line of the amplifiers, respectively. The reference lines of these amplifiers were connected with a reference electrode; (c) schematic diagram of the local-differential recording. The core electrode was connected with the signal line of the amplifier, while the shell electrode was connected with the reference line.

(Fig. 1c).

2. Materials and methods

2.1. Device fabrication

Fig. 2a schematically illustrates the process of the core–shell electrode device. We began the process with a silicon (Si) (111) substrate (n-type with a resistivity of < 3000 Ω·cm) with a thickness of 525 μm. First, the Si substrate was thermally oxidized to form 1-μm thick silicon dioxide (SiO_2), which was then patterned to expose the substrate for the patterning of catalytic gold (Au) dots (6 μm in diameter and 200 nm in thickness) via the lift-off process. Au-catalyzed VLS growth of the Si needle was carried out to form a cone-liked 240-μm long vertical needle with a tip diameter of 4 μm and a bottom diameter of 25 μm (Fig. 2a1) [14]. The VLS growth with a gas source of Si_2H_6 also caused additional depositions of poly-Si over both the Si needle and the substrate (SiO_2) [15]. Reactive ion etching was used to remove the poly-Si layer over the substrate, while the Si needle was tapered and the dot of Au-Si at the needle's tip was removed. For the electrical insulation of the Si needle, 1-μm thick SiO_2 was deposited via plasma-enhanced chemical vapor deposition (PECVD) (Fig. 2a2). Au (200 nm) was formed as the core metal of the needle with a binding layer of titanium (Ti) (30 nm), using sputtering and a subsequent lift-off process (Fig. 2a3). An interlayer parylene-C insulator (1 μm) was then formed over the core metal by vacuum deposition equipment (model PDS2010, LABCOTER) with an amount of parylene dimer (1.8 g), and the layers over both the needle tip and contact pad portions were simultaneously exposed via oxygen (O_2) plasma treatment with a spray-coated photoresist mask (Fig. 2a4). To form the shell metal of the needle, another Au/Ti (200 nm/30 nm) was formed via sputtering and subsequent wet etching (aqua regia) (Fig. 2a5). Finally, the needle and the substrate were again insulated with parylene-C (1 μm), with the exception of the needle tip and pad portions, which underwent subsequent O_2 plasma etching (Fig. 2a6).

Fig. 2b–d shows the scanning electron microscopy (SEM) images and schematic diagram of the fabricated coaxial microneedle-electrode. The diameter of the core electrode is 4 μm, while the outer diameter of the overall needle is 10 μm, and the needle length is 240 μm. Exposed heights of the core electrode and that of the shell electrode from these insulators are 4 μm and 2 μm, respectively, while the height of the insulator between the electrodes is 6 μm. Fig. 2e and Fig. 2f present a schematic diagram and SEM images of the cross-sectional view of a fabricated coaxial needle electrode prepared via the focused ion beam (FIB) technique. The SEM images indicate the conformal layer-by-layer coatings of the Au core and shell electrodes with parylene-C insulators over the Si microneedle.

2.2. In vivo recordings

The neuronal recording capability of both the core and the shell electrode in individual coaxial needles was confirmed through *in vivo* neuronal recording involving a mouse. All experimental procedures using animals were approved by the Committee for the Use of Animals at Toyohashi University of Technology, and all animal care procedures followed the Standards Relating to the Care and Management of Experimental Animals (Notification No. 6, 27 March 1980 of the Prime Minister's Office of Japan).

The coaxial needle-electrode device was packaged with flexible printed circuit (FPC) and attached to a micromanipulator (MO-10, Narishige) to control needle placement. The recording sites were stereotaxically defined, after which the coaxial electrodes were penetrated into the mouse's brain, with an optical microscope used to confirm that the needle was fully penetrated into the brain tissue. The coaxial microneedle-electrode demonstrated no fragility nor any degradation of the Si needle body or any film layer (core and shell electrodes and insulating layers) after penetration was performed seven times. During the recording, specific mouse whiskers were physically stimulated with an electromagnetic vibrator driven by electrical pulses (1 ms in duration) to activate neurons at the primary somatosensory field (S1B), while the cortical surface was kept wet through the dropwise addition of saline.

For the somatosensory response recordings, the coaxial electrode was stereotaxically penetrated into the barrel field in the S1B. As a signal reference electrode, a stainless-steel screw was drilled into the skull over the visual cortex (V1) on the left hemisphere. Following needle penetration, the principal whiskers of the mouse were mechanically stimulated by an electromagnetic vibrator to activate the S1B neurons. The simulation was controlled by a digital signal processing module (RZ2, Tucker-Davis Technologies).

In the signal acquisition and processing procedure, signals recorded from the microneedles were differentially amplified (ZC64, Tucker-Davis Technologies, 1×10^{14} Ω input impedance) with filters (0.35 Hz

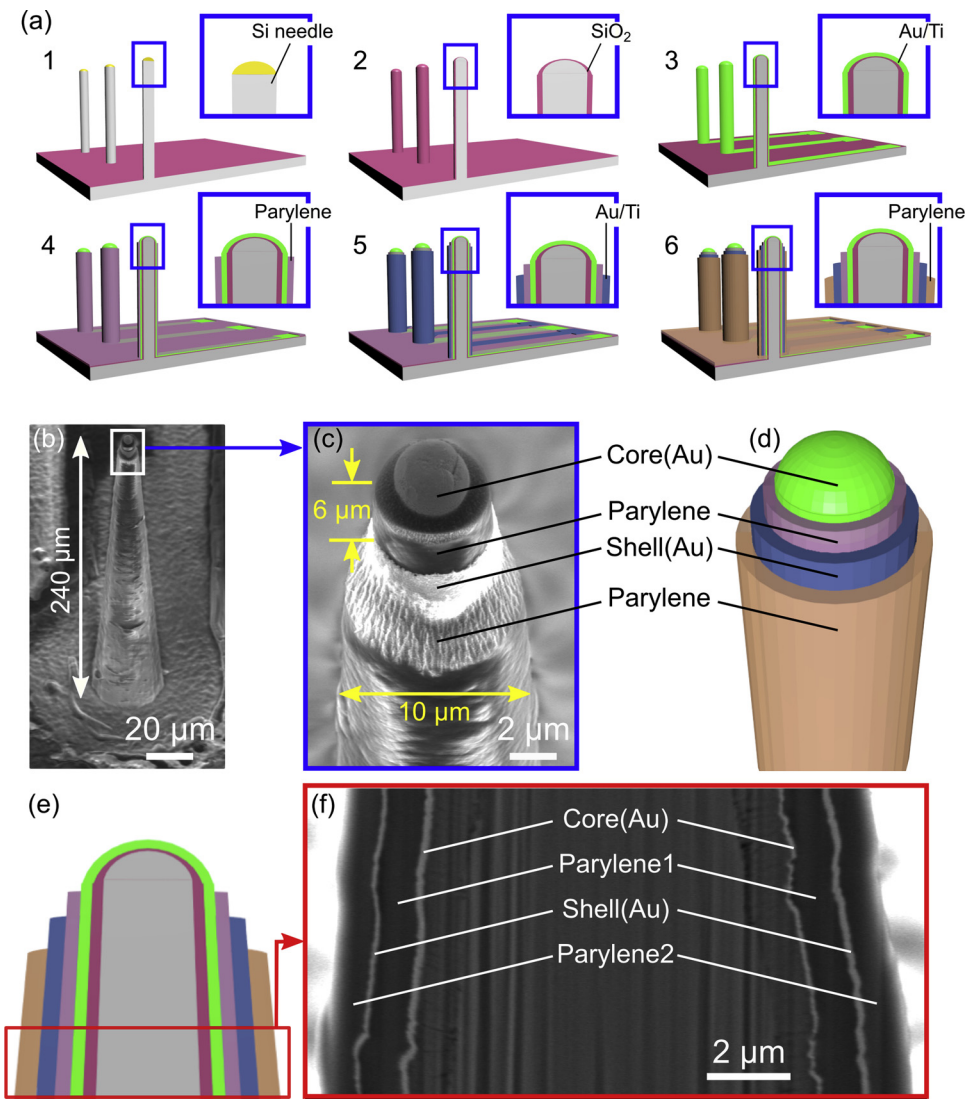

Fig. 2. Fabrication of the coaxial microneedle-electrode device. (a) Device fabrication steps: (1) VLS growth of Si-microneedle; (2) deposition of a 1-μm thick SiO_2 via PECVD; (3) sputtering of an Au layer with a Ti adhesion layer and subsequent patterning using the lift-off process to form the core electrode; (4) electrical insulation of the core electrode with a 1-μm thick parylene-C layer, and plasma etching of the parylene layer over both the needle-tip and the bonding pad; (5) sputtering of further Au/Ti layers and the subsequent wet etching to form the shell electrode; (6) device insulation with 1-μm thick parylene-C and subsequent exposure of the needle-tip and the bonding pad through plasma etching. (b) SEM image of the fabricated coaxial microneedle-electrode. The needle has a length of 240 μm. (c, d) SEM image and schematic of the tip portion of the needle. The diameter of the core electrode is 4 μm. The outer diameter of the overall needle is 10 μm. The height of the core electrode and that of the shell electrode exposed from each parylene insulator are 8 μm and 4 μm, respectively. The height of the insulator between these electrodes is 6 μm. (e) Cross-sectional schematic of the fabricated coaxial electrode. (f) SEM image of the cross-sectional view of the needle electrode prepared using FIB, showing the core and shell electrode layers of Au and the parylene-C insulator layers.

for low-cut-off and 7.5 kHz for high-cutoff). Following signal amplification, the signals were routed to a preamplifier/digitizer (PZ2, Tucker-Davis Technologies) and a digital signal processing module (RZ2, Tucker-Davis Technologies). All digital data were then stored on a hard disk in a Windows PC with a sampling frequency of 25 kHz.

3. Results

3.1. Electrical characterisations

Fig. 3a shows the impedance characteristics of the fabricated core–shell electrode. The impedance magnitudes of the core and the shell electrodes were measured in phosphate-buffered saline (PBS) at a neuronal activity frequency of 1 Hz – 10 kHz, and the results ranged from 490 MΩ to 5.9 kΩ (2.8 MΩ at 1 kHz) and from 620 MΩ to 5.6 kΩ (3.6 MΩ at 1 kHz), respectively. The average and standard deviations of both impedance characteristics were then taken from six samples (six needles from three chip devices). These values represent metal-electrolyte interfacial impedance depending on each electrode's area. The height of the core electrode exposed from the parylene-C insulating layer was 4 μm, which resulted in an electrode opening area of 150 μm^2. Meanwhile, the shell electrode had an exposed area of 100 μm^2 (2 μm in height). Due to the difference in electrode area, the core electrode exhibited a smaller impedance magnitude than the shell electrode.

Fig. 3b shows the output/input (O/I) signal amplitude ratios of the

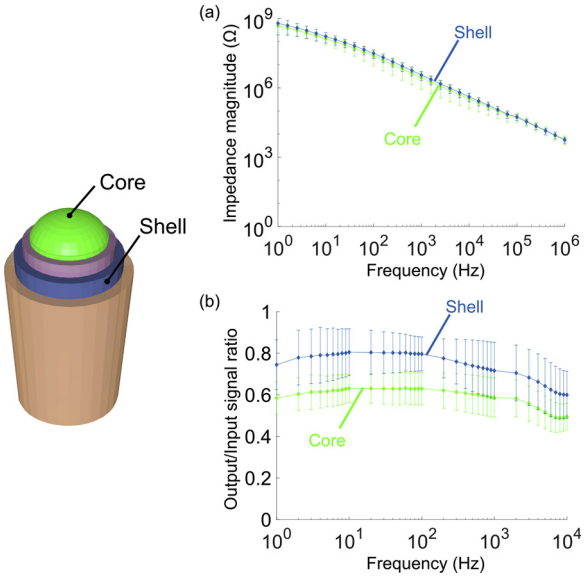

Fig. 3. Electrical characteristics of the fabricated coaxial microneedle-electrode device. (a) Impedance magnitudes of the core electrode and the shell electrode measured in PBS at 1 Hz – 10 kHz; (b) O/I signal amplitude ratios of the core and the shell electrodes measured in PBS at 1 Hz – 10 kHz.

fabricated core–shell electrode. The O/I ratios of the core and the shell electrodes were measured in saline at 1 Hz – 10 kHz, and the results ranged from 62.4%–50.6% (57.3 % at 1 kHz) and from 65.3%–49.1% (59.8 % at 1 kHz), respectively. The amplitude attenuations of these electrodes at ~100–1000 Hz were due to the electrode's impedance and the parasitic capacitances. The capacitances were included by an insulating parylene-C layer (1-μm thick) between the device interconnection (Au-Ti) and the saline solution, and an insulating SiO_2 layer (1-μm thick) between the device interconnection and the Si substrate. These capacitances resulted in a low-pass filter configuration in the recording system [10–12,16].

3.2. In vivo neuronal signal recordings

3.2.1. Multichannel recording

Here, we used a mouse weighting 25.7 g that was anesthetized through intraperitoneal injection with a urethane solution (0.5 % chlorprothixene 0.26 mL [0.10 mL/10 g] and 0.13 mL urethane [0.051 mL / 10 g]). After the head of the mouse was fixed with a stereotaxic apparatus (SR-50, Narishige, Tokyo, Japan), parts of the cranium and the dura mater of the mouse were removed before the needle-electrodes were placed over the cerebral cortex and inserted at the S1B (−1 mm posterior and 3 mm lateral to the bregma) on the right hemisphere via the fenestrae in the cranium and dura matter (Fig. 4a–c). Due to the small geometry of each needle electrode of < 10 μm in diameter, our needle provides the advantage of a low invasive electrode penetration. Fig. 4d shows photographs corresponding to the tissue area before and after the needle penetration. We observed no significant bleeding associated with the needle penetration.

Fig. 4e1 and Fig. 4f1 show LFP (3rd Butterworth filter [50–300 Hz]) simultaneously recorded via the core and shell electrodes of the microneedle (Ch. 1 in Fig. 4c), respectively. These LFPs emerged in response to the whisker stimuli with a latency of ~20 ms. The amplitudes of these recorded signals were ~800 μV for the core electrode and ~830 μV for the shell electrode (n = 100 trials). Fig. 4e2 and Fig. 4f2 show unit-activity band potential (2nd Butterworth filter [500 – 3000 Hz]) via the core and shell electrodes, respectively. Meanwhile, Fig. 4e3 and Fig. 4f3 show the raster plots and Fig. 4e4 and Fig. 4f4 show the peri-stimulus time histograms (PSTHs) for 100 trials. Spike detection of these signals was performed based on triggering of thresholds for four standard deviation (σ) of the mean signal during 0.5–1.0 s before stimulation onset. These signal waveforms of both LFP and unit-activity via the fabricated coaxial microneedle-electrode were similar to that of signals recorded via conventional tungsten electrodes and our prior micro/nanoscale needle-electrode devices [10,13] using the same recording system, as outlined in Section 2. In addition, given that these sensory responses appeared at ~20 ms following the stimulation were consistent with the reported latency in whisker stimulation of mouse [11]. Thus, these signals recorded via the core and the shell electrodes were neurophysiological responses evoked by the whisker stimuli.

To further analyze these signals, we used a peak-to-peak amplitude distribution of the spike signals simultaneously recorded via the core electrode and the shell electrode (Fig. 4g). Due to the 6-μm-gap between the core and the shell electrodes, correlation coefficient taken from the diagram was 0.793, while the other correlation coefficient of signals via the other coaxial needle in prior session was 0.944 (data not shown). These results suggested that multichannel recordings of the fabricated coaxial needle electrodes yielded no significant differences in neuronal signal between the core and the shell electrodes.

3.2.2. Local-differential recording

To achieve the differential recording of neuronal activities at the localized region within the tissue, the shell electrode was used to play the role of local-reference electrode by connecting it to the reference line of the differential amplifier. This recording configuration enables us to cancel out ambient noise. Namely that, once the needle's tip locates near a neuron, signals of the neuron via the core electrode will be enhanced, while signals via the shell electrode will be decreased.

Fig. 5a shows the signal waveforms recorded with the differential measurement configuration of the coaxial needle electrode. Similar to the multichannel recording, the same bandpass filters (50–300 and 500–3000 Hz) were used to obtain LFPs and spikes in the recording. To investigate the effects of the local-reference electrode on the recorded neuronal signals, the local-differential recording session was carried out immediately after the multichannel recording (Fig. 4), with the connection of the shell electrode changed but the recording site of the needle within the tissue left unchanged. As expected, the local-differential recording resulted in the disappearance of the LFPs, which reflected collective transmembrane currents from multiple neurons around the needle, as was confirmed through a comparison with the multichannel recording (Fig. 4e1). However, the appearance of spike signals continued when using the same bandpass filter.

For the quantitative comparison, these spike signals were further analyzed using SNR (Fig. 5b1). The SNR was defined as the peak-to-peak amplitude of the mean waveform 0.005 to 0.05 s after the stimulus onset divided by the root-mean-square signals 0 to 0.05 s before the stimulus onset. The calculated SNR of the local-differential recording was 10 ± 0.6 (mean ± SD) dB, while the multichannel recording (core electrode) degraded the SNR to 6.6 ± 2.0 (mean ± SD) dB. The improvement in SNR with the local-differential recording was due to the reduction in common mode noise with the referenced shell electrode, while the signal amplitude via the core electrode was slightly attenuated with the capacitance of the parylene-C between the core electrode and the shell electrode.

Fig. 5b2 shows a comparison of the firing rate of the multichannel recording and that of the local-differential recording. Here, the local-differential recording had a firing rate of 570 ± 60 (mean ± SD) spikes/s, which was around double that of the core electrode in the multichannel recording (the shell electrode electrically floated) (225 ± 150 [mean ± SD] spikes/s). This improvement in firing rate necessitates further discussion of the effect of the shell electrode (reference electrode) in the recording. Given that the reference electrode was closed to the signal line of the core electrode, the difference in neuronal signal between the target neurons near the core electrode and those around the needle can be enhanced. Meanwhile, the positioning of a reference electrode far from the core electrode (signal line) will result in the degradation of the difference in the neuronal signals. In the multichannel recording with the floating shell electrode (Fig. 4), we used the 1-mm diameter reference electrode screwed into the skull at the left hemisphere (V1), which was ~4-mm far positioned from the core electrode. Meanwhile, the distance between the core and the shell (reference) electrodes in the local-differential recording was 6 μm. Further, the reduction of the common mode noise by the referenced shell electrode also contributed to the improved firing rate in the differential recording.

The coaxial needle electrode also allowed for a local ground (GND) electrode to be used in the recording by connecting the shell electrode to the GND line (Fig. S1). Similar to the local-differential recording (Fig. 5a), the amplitudes of the spike signals were attenuated with the capacitance of the parylene-C insulator between the core electrode and the shell electrode. However, the noise level in the recording increased from that of the local-differential recording. Consequently, the SNR and firing rate of the shell grounded recording were 7.3 ± 0.3 (mean ± SD) dB and 273 ± 30 (mean ± SD) spikes/s, respectively, which were degraded from those of the local-differential recording.

4. Discussion

We fabricated coaxial needle-electrode, which consists of a core electrode in the needle surrounded by another shell electrode. Recording sites of electrodes were positioned at the tip portion of each needle, enabling these electrodes to be placed close to the target

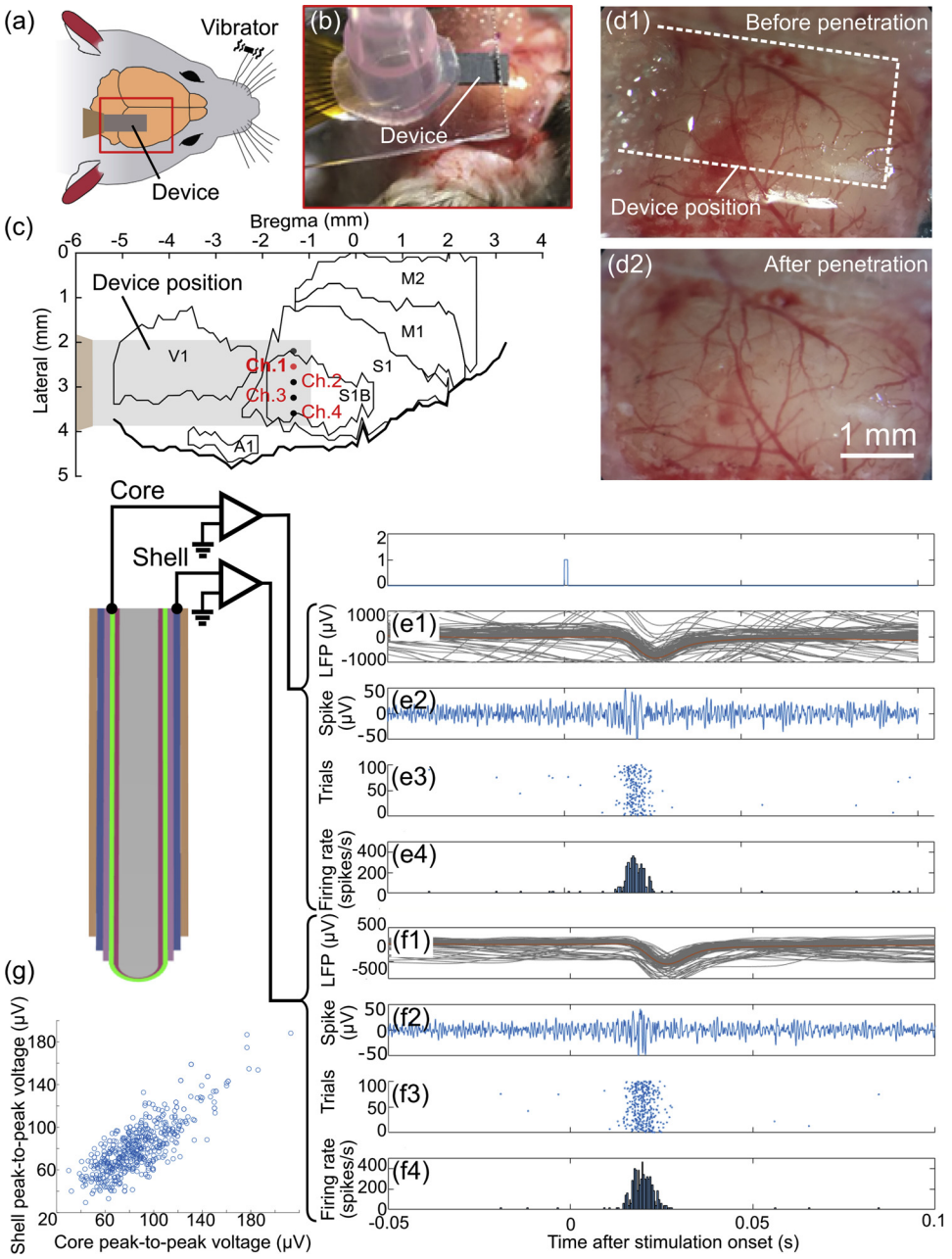

Fig. 4. Multichannel neuronal recording via coaxial microneedle-electrodes using a mouse *in vivo*. (a, b) Schematic and photograph of the coaxial electrode device placed over the mouse cortex. (c) Illustration showing the position of the coaxial electrodes. The coaxial electrodes were penetrated into the primary somatosensory cortex barrel field (S1B). The mouse's whiskers were physically stimulated with an electromagnetic vibrator driven by electrical pulses (1 ms in duration). (d1, d2) Photographs of the tissue area before and after the needle penetration: (d1) before and (d2) after the penetration of coaxial microneedle-electrodes. (e1–e4) Recorded signals via the core electrode in an electrode Ch. 1 in the array: (e1) waveform signals using a bandpass filter (3rd Butterworth filter [50–300 Hz]); (e2) a single trial signal in recordings for 100 trials using a bandpass filter (2nd Butterworth filter [500–3000 Hz]); and (e3, e4) raster plots and PSTH taken from the signals (500–3000 Hz) using detection amplitude thresholds of 4σ of the mean signal during 0.5 to 1.0 s before stimulation onset. (f1–f4) Simultaneously recorded signals via the shell electrode: f1) waveform signals using a bandpass filter (3rd Butterworth filter [50–300 Hz]); (f2) a single trial signal in recordings for 100 trials using a bandpass filter (2nd Butterworth filter [500–3000 Hz]); (f3 and f4) raster plots and PSTH taken from the signals (500–3000 Hz) using the 4 σ detection amplitude thresholds. (g) Peak-to-peak amplitude distribution of these spike signals recorded via the core electrode and the shell electrode, using the same detection threshold of 4 σ during the latency of 0.014 – 0.03 s.

neurons. This electrode's coaxial geometry will also give the high-quality signal acquisition, such as single-unit isolation from recorded signals. As demonstrated in this study, the shell electrode, which surrounds the core electrode, contributed to the suppression of signals outside of the shell electrode, while the core electrode in the needle detected the neuronal signals near the recording site.

The device was batch fabricated by VLS growth of Si needles and photolithography-based microfabrication processes. We performed the device fabrication using our in-house clean room process. The clean room allows for MOSFET device fabrication, which enables us to further integrate coaxial microneedle electrodes with circuitry by fabricating MOSFETs prior to the VLS growth of the silicon needles [17–19]. Advantage of the batch fabrication process of multiple needle-electrodes is to provide consistent geometries of electrodes between needles. As confirmed in the electrical characterisations of fabricated devices, no significant differences in impedance and OI ratio between needles were observed (Fig. 3). The results suggested that each needle has similar opening areas of core electrode and shell electrode in individual needles. Due to the small opening area (88 – 103 μm^2) and the material of Au, these electrodes showed impedance magnitudes of > 2 MΩ at 1 kHz. To reduce these impedances of electrode with the small recording area, a way is to use a low impedance material, including PEDOT [20–23] platinum black [10,11,24] and iridium oxide [25,26]. We have confirmed the impedance reduction of < 10-μm-diameter needle-electrode by electroplating modification with platinum black [10,11]. However, the electroplating process, which was carried out for electrodes one by one, caused electrical property fluctuation between the needles. In addition to the electrical property fluctuation, the plating of additional material to each needle-electrode increases the geometry of the recording site. Compared to the electroplating process, the proposed coaxial needle-electrode, which provides the local-differential recording configuration, improved the signal quality in the neuronal recording without additional coating of the low impedance materials.

An important characteristic of the coaxial microneedle-electrode relates to crosstalk, which is caused by facing the two electrodes with the insulating layer. The crosstalk-associated impedance between the

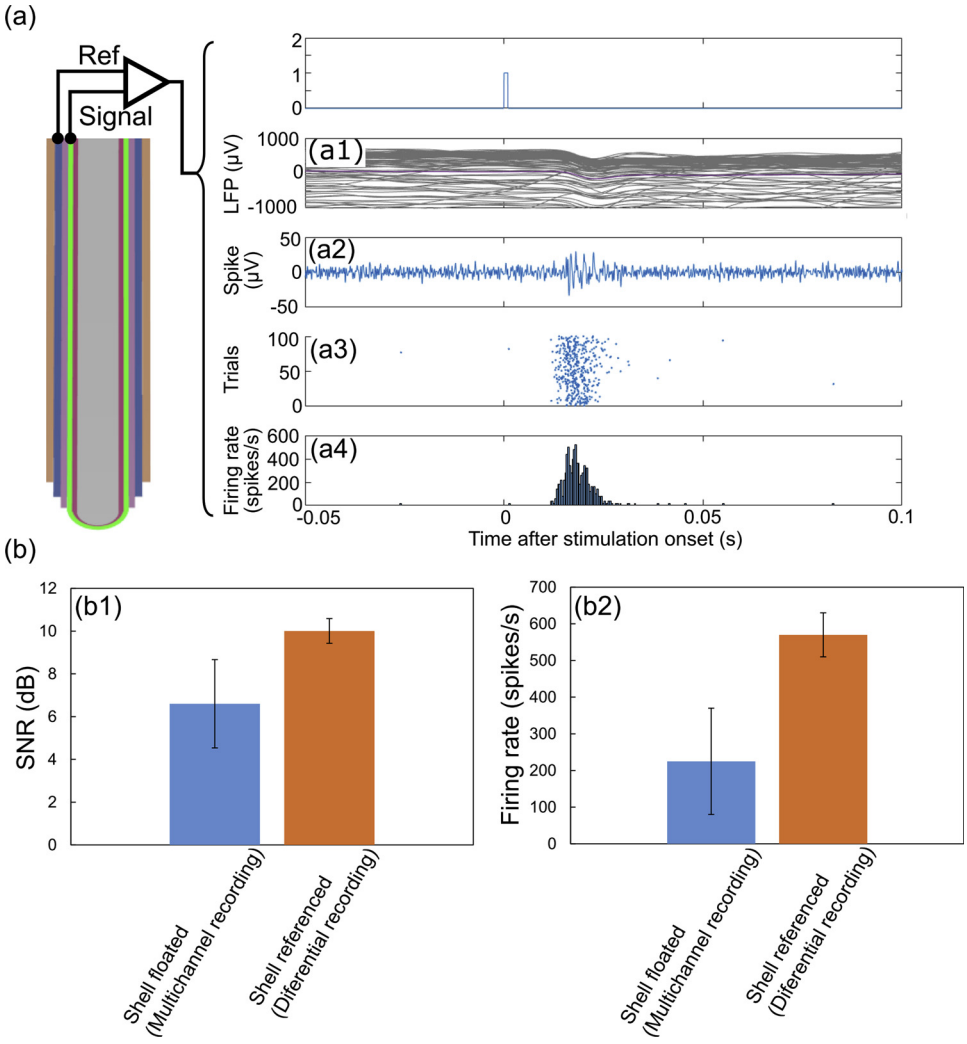

Fig. 5. Local-differential neuronal recording using a mouse *in vivo*. (a) Schematic of the recording configuration. The recording was conducted by connecting the shell electrode to the reference line of the differential amplifier, without changing the needle position from the multisite recording (Fig. 4). (a1) Waveform signals using a bandpass filter (3rd Butterworth filter [50–300 Hz]); (a2) a single trial signal in recordings (100 trials) using a bandpass filter (3nd Butterworth filter [500–3000 Hz]); and (a3, a4) raster plots and PSTH taken from the signals (500–3000 Hz) using detection amplitude thresholds of 4σ of the mean signal during 0.5 to 1.0 s before stimulation onset. (b) Comparison of the neuronal recording signals of the multisite recording (shell electrode floated) and the differential recording (shell electrode referenced). (b1) SNRs and (b2) firing rates in the comparison. Averages and standard deviations of both SNR and firing rate were taken from two samples.

core electrode and the shell electrode measured at 1 kHz was 62.3 MΩ (Fig. S2), which was over 17 times larger than that of each electrode (e.g., 3.6 MΩ for the shell electrode, Fig.3a). The crosstalk was mainly dominated by the device's interconnections, which were designed from the needle-site to the bonding pad (4000 μm in length and 60 μm in width for each interconnection). The device interconnections for the core electrode and the shell electrode were stacked with an insulating layer of 1-μm thick parylene-C between them. While the measured crosstalk had a high enough impedance for our recording, the crosstalk could be reduced by increasing the thickness of the insulating layer.

We demonstrated multichannel neuronal recording via the coaxial microneedle electrode, in which the gap between the core and the shell electrode in the present design was 6 μm (Fig. 2c). A more significant difference in neuronal activities between electrodes could be obtained by increasing the electrode gap in the device fabrication (> 6 μm) (e.g., ~80-μm peak amplitude difference via a four-core electrode [27], 25-μm center-to-center recording-site spacing [5]). The electrode gap can be increased by increasing the exposure process of shell-electrode layer of Au/Ti (Figs. 2 5–6). In addition to the multichannel recording at the local area, the coaxial needle-electrode will provide the multichannel recording from different cortical layers by designing electrode positions in the needle consistent with depths of these cortical layers (e.g., ~ 200 μm and ~400 μm for cortical layers of 2/3 and 4 of mouse, respectively [28]). Although the length of fabricated needles was set at 240 μm for the mouse's cortical 2/3 layer, the needle length can further be increased by VLS growth of Si-needle (e.g., 400 μm [13] and 1 mm [10]. The proposed coaxial needle process will also allow us to design additional layers of shell electrode, increasing the number of recording sites more than two channels. Formation of each shell electrode could induce a ~2.5 μm increase in the overall needle-dimeter (thicknesses of Au/Ti shell-electrode layers and inter parylene-C insulator were 230 nm and 1 μm, respectively, Fig. 2f).

We performed both multichannel and differential *in vivo* acute recordings using mice, in which parts of the cranium and dura mater of the mice were removed for needle penetration. Although we did not investigate any infectious diseases associated with the device, infection risk must be addressed for future chronic recording applications. We are currently working on device implantation, which will allow for long-period neuronal recordings in mice with minimum damage to brain tissues.

Other application of the proposed coaxial microneedle-electrode includes neural stimulation. Because the fabricated microneedle consists of two channel electrodes (core and shell), this needle device will provide the neuronal stimulation can be conducted at the local area within the tissue. The needle technology is also applicable to multichannel recording from different cortical columns. The fabricated device had a linear array of four needles spaced at 150 μm intervals. We also analyzed the neuronal signals recorded via the other coaxial needle-electrode (Ch. 4 in Fig. 4c), in which the needle also detected similar neuronal signals to Ch. 1 (Figs. 4e-f and 5). The spacing can further be reduced by the photolithography-based fabrication process, while the number of needles increases, providing the high spatial recording of neuronal activities with high quality signals.

5. Conclusion

In this study, we proposed a coaxial cable–inspired microneedle-electrode device to explore potential improvements in the quality of the electrophysiological recording using microelectrodes. The fabrication of the coaxial microneedle-electrode was based on a VLS-grown silicon microneedle and the subsequent layer-by-layer formation of metal and insulating layers to realize the core and shell electrodes for individual needles with < 10-μm diameter. This needle geometry offers no major traumatic injury in a tissue [8,9], while larger diameter needles induce obvious tissue damage (disruption of local communication between glial by > 20-μm-needle and blood–brain barrier breach by ~ 50-μm needle). The neuronal recording capability of the fabricated electrode device was confirmed by conducting multichannel recording via the core electrode and the shell electrode using a mouse *in vivo*. We have confirmed this specific advantage of the coaxial microneedle electrode by conducting differential recordings. Connecting the shell electrode to the reference line of the amplifier yielded a differential recording at the localized region within the tissue, which resulted in an improvement in terms of SNR and firing rate in the recording. To the best of our knowledge, no one has demonstrated such differential recordings and observed similar improvements in the signal quality of neuronal recordings. As demonstrated in this paper, the coaxial microneedle-electrode will contribute to improving electrophysiological recordings including *ex vivo* and *in vitro* applications, similar to the *in vivo* recording, offering the possibility of recording neuronal activities with high-quality signals.

CRediT authorship contribution statement

Shinnosuke Idogawa: Conceptualization, Methodology, Investigation, Writing - original draft, Writing - review & editing. **Koji Yamashita:** Methodology, Investigation. **Yoshihiro Kubota:** Investigation. **Hirohito Sawahata:** Methodology, Investigation. **Rioki Sanda:** Methodology. **Shota Yamagiwa:** Investigation. **Rika Numano:** Writing - original draft, Writing - review & editing. **Kowa Koida:** Writing - original draft, Writing - review & editing. **Takeshi Kawano:** Supervision, Writing - original draft, Writing - review & editing, Funding acquisition.

Declaration of Competing Interest

The authors declare that they have no known competing financial interests or personal relationships that could have appeared to influence the work reported in this paper.

Acknowledgements

This work was supported by JSPS KAKENHI (No. 17H03250, No. 26709024, and No. 20H00244), Strategic Advancement of Multi-Purpose Ultra-Human Robot and Artificial Intelligence Technologies program from NEDO, and Nagai Foundation for Science & Technology. R.N. was supported by Takeda Science Foundation. K.K. was supported by JSPS KAKENHI (No. 15H05917).

Appendix A. Supplementary data

Supplementary material related to this article can be found, in the online version, at doi:https://doi.org/10.1016/j.snb.2020.128442.

References

[1] D.H. Kim, J. Viventi, J.J. Amsden, J. Xiao, L. Vigeland, Y.S. Kim, J.A. Blanco, B. Panilaitis, E.S. Frechette, D. Contreras, D.L. Kaplan, F.G. Omenetto, Y. Huang, K.C. Hwang, M.R. Zakin, B. Litt, J.A. Rogers, Dissolvable films of silk fibroin for ultrathin conformal bio-integrated electronics, Nat. Mater. 9 (2010) 511–517, https://doi.org/10.1038/nmat2745.

[2] G. Buzsáki, C.A. Anastassiou, C. Koch, The origin of extracellular fields and currents-EEG, ECoG, LFP and spikes, Nat. Rev. Neurosci. 13 (2012) 407–420, https://doi.org/10.1038/nrn3241.

[3] C. Mora Lopez, J. Putzeys, B.C. Raducanu, M. Ballini, S. Wang, A. Andrei, V. Rochus, R. Vandebriel, S. Severi, C. Van Hoof, S. Musa, N. Van Helleputte, R.F. Yazicioglu, S. Mitra, A neural probe with up to 966 electrodes and up to 384 configurable channels in 0.13 μm SOI CMOS, IEEE Trans. Biomed. Circuits Syst. 11 (2017) 510–522, https://doi.org/10.1109/TBCAS.2016.2646901.

[4] S. Wang, C.M. Lopez, S.K. Garakoui, H. Chun, D.G. Salinas, W. Sijbers, J. Putzeys, E. Martens, J. Craninckx, N. Van Helleputte, A compact quad-shank CMOS neural probe with 5,120 addressable recording sites and 384 fully differential parallel channels, IEEE Trans. Biomed. Circuits Syst. 13 (2019) 1625–1634, https://doi.org/10.1109/TBCAS.2019.2942450.

[5] J.J. Jun, N.A. Steinmetz, J.H. Siegle, D.J. Denman, M. Bauza, B. Barbarits, A.K. Lee, C.A. Anastassiou, A. Andrei, Ç. Aydin, M. Barbic, T.J. Blanche, V. Bonin, J. Couto, B. Dutta, S.L. Gratiy, D.A. Gutnisky, M. Häusser, B. Karsh, P. Ledochowitsch, C.M. Lopez, C. Mitelut, S. Musa, M. Okun, M. Pachitariu, J. Putzeys, P.D. Rich, C. Rossant, W.L. Sun, K. Svoboda, M. Carandini, K.D. Harris, C. Koch, J. O'Keefe, T.D. Harris, Fully integrated silicon probes for high-density recording of neural activity, Nature. 551 (2017) 232–236, https://doi.org/10.1038/nature24636.

[6] T. Saxena, L. Karumbaiah, E.A. Gaupp, R. Patkar, K. Patil, M. Betancur, G.B. Stanley, R.V. Bellamkonda, The impact of chronic blood–brain barrier breach on intracortical electrode function, Biomaterials. 34 (2013) 4703–4713, https://doi.org/10.1016/J.BIOMATERIALS.2013.03.007.

[7] D.H. Szarowski, M.D. Andersen, S. Retterer, A.J. Spence, M. Isaacson, H.G. Craighead, J.N. Turner, W. Shain, Brain responses to micro-machined silicon devices, Brain Res. 983 (2003) 23–35, https://doi.org/10.1016/S0006-8993(03)03023-3.

[8] D.J. Edell, V. Van Toi, V.M. Mcneil, L.D. Clark, Factors influencing the biocompatibility of insertable silicon microshafts, Cereb. Cortex 39 (1992) 635–643.

[9] T.D. Yoshida Kozai, N.B. Langhals, P.R. Patel, X. Deng, H. Zhang, K.L. Smith, J. Lahann, N.A. Kotov, D.R. Kipke, Ultrasmall implantable composite microelectrodes with bioactive surfaces for chronic neural interfaces, Nat. Mater. 11 (2012) 1065–1073, https://doi.org/10.1038/nmat3468.

[10] A. Fujishiro, H. Kaneko, T. Kawashima, M. Ishida, T. Kawano, In vivo neuronal action potential recordings via three-dimensional microscale needle-electrode arrays, Sci. Rep. 4 (2014), https://doi.org/10.1038/srep04868.

[11] H. Sawahata, S. Yamagiwa, A. Moriya, T. Dong, H. Oi, Y. Ando, R. Numano, M. Ishida, K. Koida, T. Kawano, Single 5 μm diameter needle electrode block modules for unit recordings in vivo, Sci. Rep. 6 (2016), https://doi.org/10.1038/srep35806.

[12] Y. Kubota, H. Oi, H. Sawahata, A. Goryu, Y. Ando, R. Numano, M. IShida, T. Kawano, Nanoscale-tipped high-aspect-Ratio vertical microneedle electrodes for intracellular recordings, Small. 12 (2016) 2846–2853, https://doi.org/10.1002/smll.201600172.

[13] Y. Kubota, S. Yamagiwa, H. Sawahata, S. Idogawa, S. Tsuruhara, R. Numano, K. Koida, M. Ishida, T. Kawano, Long nanoneedle-electrode devices for extracellular and intracellular recording in vivo, Sensors Actuators B Chem. 258 (2018) 1287–1294, https://doi.org/10.1016/j.snb.2017.11.152.

[14] A. Ikedo, T. Kawashima, T. Kawano, M. Ishida, Vertically aligned silicon microwire arrays of various lengths by repeated selective vapor-liquid-solid growth of n-type silicon/n-type silicon, Applied Physics Letters 95 (2009), https://doi.org/10.1063/1.3178556.

[15] T. Kawano, Y. Kato, M. Futagawa, H. Takao, K. Sawada, M. Ishida, Fabrication and properties of ultrasmall Si wire arrays with circuits by vapor-liquid-solid growth, Sensors Actuators, A Phys. 97–98 (2002) 709–715, https://doi.org/10.1016/S0924-4247(02)00008-0.

[16] T. Harimoto, K. Takei, T. Kawano, A. Ishihara, T. Kawashima, H. Kaneko, M. Ishida, S. Usui, Enlarged gold-tipped silicon microprobe arrays and signal compensation for multi-site electroretinogram recordings in the isolated carp retina, Biosens. Bioelectron. 26 (2011) 2368–2375, https://doi.org/10.1016/j.bios.2010.10.014.

[17] T. Kawano, Y. Kato, R. Tani, H. Takao, K. Sawada, M. Ishida, Selective vapor-liquid-Solid epitaxial growth of Micro-Si probe electrode arrays with on-chip mosfets on Si (1 1 1) substrates, IEEE Trans. Electron Devices 51 (2004) 415–420, https://doi.org/10.1109/TED.2003.822473.

[18] T. Kawano, T. Harimoto, A. Ishihara, K. Takei, T. Kawashima, S. Usui, M. Ishida, Electrical interfacing between neurons and electronics via vertically integrated sub-4mu;m-diameter silicon probe arrays fabricated by vapor-liquid-solid growth, Biosens. Bioelectron. 25 (2010) 1809–1815, https://doi.org/10.1016/j.bios.2009.12.037.

[19] A. Okugawa, K. Mayumi, A. Ikedo, M. Ishida, T. Kawano, Heterogeneously integrated vaporliquidsolid grown silicon probes/(111) and silicon MOSFETs/(100), IEEE Electron Device Lett. 32 (2011) 683–685, https://doi.org/10.1109/LED.2011.2120590.

[20] S.J. Wilks, S. Richardson-burns, J.L. Hendricks, M. David, K.J. Otto, Poly (3, 4-ethylene dioxythiophene)(PEDOT) as a micro-neural interface material for electrostimulation, Front. Neuroeng. 2 (2017), https://doi.org/10.3389/neuro.16.007.

[21] D. Khodagholy, T. Doublet, M. Gurfinkel, P. Quilichini, E. Ismailova, P. Leleux, T. Herve, S. Sanaur, C. Bernard, G.G. Malliaras, Highly conformable conducting polymer electrodes for in vivo recordings, Adv. Mater. 23 (2011) 268–272, https://doi.org/10.1002/adma.201102378.

[22] S. Venkatraman, J. Hendricks, Z.A. King, A.J. Sereno, S. Richardson-Burns, D. Martin, J.M. Carmena, In vitro and in vivo evaluation of PEDOT microelectrodes for neural stimulation and recording, IEEE Trans. Neural Syst. Rehabil. Eng. 19 (2011) 307–316, https://doi.org/10.1109/TNSRE.2011.2109399.

[23] M.R. Abidian, D.C. Martin, Multifunctional nanobiomaterials for neural interfaces, Adv. Funct. Mater. 19 (2009) 573–585, https://doi.org/10.1002/adfm.200801473.
[24] H. Oka, K. Shimono, R. Ogawa, H. Sugihara, M. Taketani, A new planar multi-electrode array for extracellular recording: application to hippocampal acute slice, J. Neurosci. Methods 93 (1999) 61–67, https://doi.org/10.1016/S0165-0270(99)00113-2.
[25] S. Yamagiwa, A. Fujishiro, H. Sawahata, R. Numano, M. Ishida, T. Kawano, Layer-by-layer assembled nanorough iridium-oxide/platinum-black for low-voltage microscale electrode neurostimulation, Sensors Actuators B Chem. 206 (2015) 205–211, https://doi.org/10.1016/j.snb.2014.09.048.
[26] S.F. Cogan, J. Ehrlich, T.D. Plante, A. Smirnov, D.B. Shire, M. Gingerich, J.F. Rizzo, Sputtered iridium oxide films for neural stimulation electrodes, J. Biomed. Mater. Res. - Part B Appl. Biomater. 89 (2009) 353–361, https://doi.org/10.1002/jbm.b.31223.
[27] H. Kaneko, H. Tamura, S.S. Suzuki, Tracking spike-amplitude changes to improve the quality of multineuronal data analysis, IEEE Trans. Biomed. Eng. 54 (2007) 262–272, https://doi.org/10.1109/TBME.2006.886934.
[28] J. DeFelipe, The evolution of the brain, the human nature of cortical circuits, and intellectual creativity, Front. Neuroanat. 5 (2011), https://doi.org/10.3389/fnana.2011.00029.

Shinnosuke Idogawa completed his B.S. degree in 2016 and M.S. degree in 2018 from the Department of Electrical and Electronic Information Engineering, Toyohashi University of Technology, Japan. He is pursuing his Ph.D. from the Department of Electrical and Electronic Engineering, Toyohashi University of Technology, Japan.

Koji Yamashita completed his B.S. degree in 2017 and M.S. degree in 2019 from the Department of Electrical and Electronic Information Engineering, Toyohashi University of Technology, Japan. He is pursuing his Ph.D. from the Department of Electrical and Electronic Engineering, Toyohashi University of Technology, Japan.

Yoshihiro Kubota completed his M.S. degree in 2015, and Ph.D. in 2018, in the Department of Electrical and Electronic Information Engineering, Toyohashi University of Technology, Japan.

Hirohito Sawahata had been a Postdoctoral Research Fellow during 2009–2012 at Graduate school of Medical and Dental sciences, Niigata University, Japan and completed his Ph.D. from Graduate School of Science and Engineering, Yamagata University, Japan. During 2012–2013 he worked as an Assistant Professor at Graduate School of Medical and Dental sciences, Niigata University, Japan. During 2013–2017, he is working as an Assistant Professor, Department of Electrical and Electronic Information Engineering, Toyohashi University of Technology, Japan. During 2017–2018, he was a Postdoctoral Research Fellow, National Institute of Advanced Industrial Science and Technology (AIST), Japan. From 2019, he was as an Assistant Professor, National Institute of Technology (KOSEN), Ibaraki College, Japan.

Rioki Sanda completed his B.S.in 2019 from Department of Electrical and Electronic Information Engineering, Toyohashi University of Technology, Japan. He is pursuing his M.S. at the same institution.

Shota Yamagiwa completed his M.S. degree in 2012, Ph.D. degree in 2016, and between 2004 and 2005, he was a Postdoctoral Research Fellow at Department of Electrical and Electronic Information Engineering, Toyohashi University of Technology, Japan. He is working as a Postdoctoral Research Fellow, Department of Electrical and Electronic Information Engineering, Toyohashi University of Technology, Japan.

Rika Numano completed her B.Sc. in 1996, M.Sc. in 1998, and Ph.D. in 2002, all from Faculty of Technology, University of Tokyo, Japan. She was a Postdoctoral Research Fellow (Japan Society for the Promotion of Science), Human Genome Center Institute of Medical Science, University of Tokyo, Japan between 2002 and2005, Postdoctoral Fellow (Japan Society for the Promotion of Science Postdoctoral fellowship for research abroad), Department of Molecular and Cell Biology, University of California Berkeley between 2005 and 2006, a researcher, Cell Function Dynamics, RIKEN between 2006 and 2007, a Researcher, ERATO Project, Japan Science and Technology Agency between 2007 and 2010 and Tenure-truck Associate professor, Electronics-Inspired Interdisciplinary Research Institute (EIIRIS),Toyohashi University of Technology, between 2010 and 2013. Currently, from 2013, she is working as an Associate professor, at Department of Environmental and Life Sciences, Toyohashi University of Technology, Japan.

Kowa Koida completed his Ph.D. degree, Interdisciplinary Graduate School of Science and Engineering, Tokyo Institute of Technology, Japan in 2000. He had been a Postdoctoral Research Fellow during 2000–2007 at National Institute for Physiological Sciences, Japan. During 2007–2010 he worked as an Assistant Professor at the same institution. He is working as an Associate professor, Department of Computer and Science and Engineering, Toyohashi University of Technology, Japan, and Electronics Inspired-Interdisciplinary Research Institute (EIIRIS) at the same University.

Takeshi Kawano completed his M.S. degree in 2001, Ph.D. degree in 2004, and between 2004 and 2005, he was a Postdoctoral Research Fellow at Department of Electrical and Electronic Engineering, Toyohashi University of Technology, Japan. During 2005–2007, he was a Postdoctoral Research Fellow (Japan Society for the Promotion of Science Postdoctoral fellowship for research abroad), Department of Mechanical Engineering, Berkeley Sensor and Actuator Center (BSAC), University of California Berkeley. During 2007–2010 was an Assistant Professor, Toyohashi University of Technology, Electrical and Electronic Engineering, Japan. From 2010 on wards he has been PRESTO Researcher, Japan Science and Technology Agency (JST) as well as an Associate Professor, Electrical and Electronic Information Engineering Toyohashi University of Technology, Japan.